



## Research article

# Zn complexed on hybrid manganese doped cobalt ferrite nanoparticles covered by silica as a catalyst in the synthesis of 2-amino-4*H*-pyran and *N*- arylquinoline derivatives

Najmieh Ahadi <sup>a</sup>, Akbar Mobinikhaledi <sup>a,b,\*</sup>, Amir Hossain Ebrahimi <sup>a</sup><sup>a</sup> Department of Chemistry, Faculty of Science, Arak University, Arak, 38156-88138, Iran<sup>b</sup> Institute of Nanosciences and Nanotechnology, Arak University, Arak, Iran

## ARTICLE INFO

## Keywords:

Magnetic nanoparticles  
Nanocatalyst  
2-Amino-4*H*-pyrans  
*N*- arylquinolines  
Green chemistry

## ABSTRACT

In the present work, Zn complexed on hybrid manganese doped cobalt ferrite nanoparticles covered by silica were synthesized. These MNPs were characterized using different techniques including Fourier-transform infrared spectroscopy (FT-IR), X-ray diffraction analysis (XRD), Field emission-scanning electron micro-scope (FE-SEM), Energy-dispersive X-ray spectroscopy (EDS), Vibration sample magnetometer (VSM), Inductively coupled plasma atomic emission spectroscopy (ICP), Zeta potential and Thermogravimetric analysis (TGA). FE-SEM Images showed uniform spherical shape with rough surfaces and an aggregation in structure of MNPs. A decrease in *M<sub>s</sub>* is visible in VSM analysis due to the increase in particle diameter as a result of loading the organic coating on the surface of the magnetic nanoparticles. According to TGA analysis, the synthesized MNPs have good stability up to 125 °C. The ICP analysis indicates the presence of 0.13 mmol/g zinc on the surface of loaded MNPs. The effect of these prepared MNPs as a catalyst was studied in the synthesis of 2-amino-4*H*-pyran and *N*- arylquinoline derivatives. This method provides excellent yield of products with short reaction time, simple purification and easy separation of the catalyst. Furthermore, the reusability of the catalyst during five periods was not associated with a significant decrease in its activity.

## 1. Introduction

2-Amino-4*H*-pyran and *N*- arylquinoline derivatives have exhibited diverse biological and pharmaceutical actions such as anti-tumor [1,2], antibacterial [3,4], anticoagulant [5], anticancer [2,6], etc. Multicomponent reactions (MCR) are known as a simple and very valuable method for the synthesis of a variety of complex organic molecules including pyran derivatives. Atomic economy, less use of solvents and chemicals, low cost, energy saving and short reaction time are some benefits of these reactions [7–9]. The easy and green preparation of 2-amino-4*H*-pyran and *N*- arylquinoline derivatives is extremely important due to their many applications. Several methods have been represented in the literature for the synthesis of 2-amino-4*H*-pyrans [10–13] and also *N*- arylquinolines [10,11]. But, some of these methods, despite having some advantages, have limitations including long reaction time, employing of toxic and costly solvents. Therefore, the synthesis of 2-amino-4*H*-pyran and *N*- arylquinoline derivatives using a cheap and green method is still extremely important for chemists. A literature search confirms the efforts of chemists in the synthesis of

\* Corresponding author. Department of Chemistry, Faculty of Science, Arak University, Arak, 38156-88138, Iran.  
E-mail address: [akbar\\_mobini@yahoo.com](mailto:akbar_mobini@yahoo.com) (A. Mobinikhaledi).

<https://doi.org/10.1016/j.heliyon.2024.e30620>

Received 26 January 2024; Received in revised form 27 April 2024; Accepted 30 April 2024

Available online 6 May 2024

2405-8440/© 2024 Published by Elsevier Ltd. This is an open access article under the CC BY-NC-ND license (<http://creativecommons.org/licenses/by-nc-nd/4.0/>).

2-amino-4H-pyran and N- arylquinoline in the presence of green and environmentally friendly conditions [12–14].

Recently, significant advances in the field of nanotechnology have led to progress and revolution in various fields, including the synthesis of organic compounds, drug delivery [15], adsorption [16], biomedical [17], engineering [18], and catalysis [19]. Among normal nanoparticles, magnetic nanoparticles have been the subject of a wide range of researches in recent years due to their distinctive characteristics, which enable their potential use in biomedicine [20], catalysis [21], and agriculture [22]. The modifying of nanoparticles and increasing their superparamagnetic property makes them easily separated from the reaction mixture by an external magnet [21]. Also, extensive surface area, thermal stability, eco-friendly and low cost, excellent recyclability and stabilization of various functional groups are among the factors that provide the design and preparation of magnetic nanoparticles as a catalyst [23].

Following our interest towards the development of new and more efficient synthetic methods for synthesis of various heterocycles using modified MNPs [24–27], we are going to offer the synthesis of a novel Zn complexed on hybrid manganese doped cobalt ferrite nanoparticles covered by silica and their usages in the synthesis of 2-amino-4H-pyran and N- arylquinoline derivatives.

## 2. Experimental

### 2.1. Material and methods

All chemicals and solvents were purchased from Merck, Fluka, and Aldrich chemical companies and used without further purification. The digital electrothermal system was utilized to determine the melting point of compounds. The progress of chemical reactions was monitored by thin-layer chromatography on UV-active aluminum-backed plates of silica gel 60 F 254. The Fourier-transform infrared spectroscopy (FT-IR spectra) were obtained on the Bruker alpha series in the 400–4000  $\text{cm}^{-1}$  using KBr pellets.  $^1\text{H}$  and  $^{13}\text{C}$  NMR spectra were recorded on the Bruker Avance spectrometer at 300 and 75 MHz, respectively using  $\text{DMSO-}d_6$  or  $\text{CDCl}_3$  as a solvent. Amount of Zn loaded on MNPs was measured by the inductively coupled plasma atomic emission spectroscopy (ICP spectrometer) (analytikjena 9100 model). The crystal structure of  $\text{MCF@SiO}_2\text{-Pr-ABT@ZnCl}_2$  MNPs was investigated by the Philips Xpert Xray powder diffraction (XRD) diffract meter via  $\text{Cu K}\alpha$  radiation ( $\lambda = 0.15406$  nm) in the range of Bragg angle  $2\theta = 10^\circ\text{--}80^\circ$ . The magnetic properties of MCF and  $\text{MCF@SiO}_2\text{-Pr-ABT@ZnCl}_2$  MNPs were evaluated using a vibrating sample magnetometer (model 730 VSM) at room temperature with applied field in the range of  $\pm 8000$  Oe. The thermogravimetric analysis (TGA) of  $\text{MCF@SiO}_2\text{-Pr-ABT@ZnCl}_2$  MNPs was carried out using a matter TA4000 system under Ar atmosphere in the range of 25–700  $^\circ\text{C}$  at a heating speed of 10  $^\circ\text{C}$  per min. Also, the morphology and the size of nanoparticles were measured on a Tescan mira II field emission-scanning electron microscope (FE-SEM). The chemical elements of the  $\text{MCF@SiO}_2\text{-Pr-ABT@ZnCl}_2$  MNPs were recognized with Elemental chemical analysis [energy-dispersive X-ray spectroscopy (EDS)] coupled with SEM. The zeta  $\text{MCF@SiO}_2\text{-Pr-ABT@ZnCl}_2$  MNPs was determined by Zeta Potential Analyzer (CAD) at  $\text{pH} = 5.5$ .

#### 2.1.1. Preparation of $\text{MnCoFe}_2\text{O}_4$ (MCF MNPs)

$\text{MnCoFe}_2\text{O}_4$  MNPs were prepared according to the literature [28]. A mixture of  $\text{Mn}^{+2}:\text{Co}^{+2}:\text{Fe}^{+3}$  with a molar ratio (1:1:4) was resolved in deionized water (100 mL) and heated at 95  $^\circ\text{C}$  for 2 h. The pH of the solution was controlled with the ammonium hydroxide (25 %) ( $\text{pH} = 12$ ) and heated for another 2 h under the same conditions. The obtained precipitate was isolated by an external magnetic field, washed several times with warm deionized water (200 mL) and ethanol (10 mL), and dried in the oven at 70  $^\circ\text{C}$ .

#### 2.1.2. Preparation of silica-coated MNPs ( $\text{MnCoFe}_2\text{O}_4\text{@SiO}_2$ MNPs) (MCF@ $\text{SiO}_2$ MNPs)

$\text{MnCoFe}_2\text{O}_4\text{@SiO}_2$  MNPs were synthesized by the Stöber method [29]. A mixture of  $\text{MnCoFe}_2\text{O}_4$  (0.5 g), deionized water (1.5 mL), ethanol (10 mL), and ammonium hydroxide (25 %) (0.4 mL) was sonicated by ultrasonic irradiation for 30 min. Subsequently, tetraethylortosilicate (TEOS, 0.4 mL) was added to the mixture and stirred for 24 h at room temperature. The magnetic residue was removed from the mixture by a magnetic field, washed with deionized water (50 mL) and ethanol (10 mL), and dried at 70  $^\circ\text{C}$ .

#### 2.1.3. Preparation of $\text{MnCoFe}_2\text{O}_4\text{@SiO}_2\text{-Pr-Cl}$ MNPs (MCF@ $\text{SiO}_2\text{-Pr-Cl}$ )

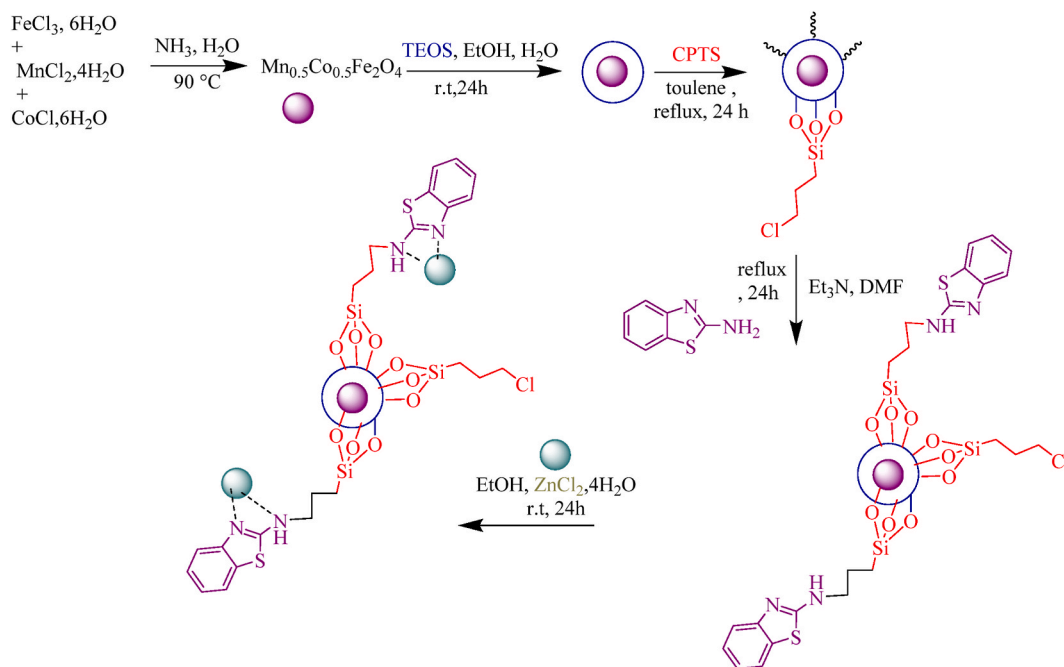
$\text{MnCoFe}_2\text{O}_4\text{@SiO}_2\text{-Pr-Cl}$  MNPs (MCF@ $\text{SiO}_2\text{-Pr-Cl}$ ) were synthesized according to our earlier report [30].  $\text{MnCoFe}_2\text{O}_4\text{@SiO}_2$  MNPs (0.5 g) was poured in a round-bottom flask (25 mL) and dispersed in 20 mL of toluene under ultrasound waves for 30 min. CPTS (1 g) was added to the mixture and refluxed for 24 h at 110  $^\circ\text{C}$ . The magnetic nanoparticles were isolated using an external magnetic field, washed with toluene (15 mL, three times) and dried at 70  $^\circ\text{C}$  without vacuum condition.

#### 2.1.4. Modification of $\text{MnCoFe}_2\text{O}_4\text{@SiO}_2\text{-Pr-Cl}$ by 2-aminobenzothiazole ( $\text{MnCoFe}_2\text{O}_4\text{@SiO}_2\text{-Pr-Benzotiazol}$ (MCF@ $\text{SiO}_2\text{-Pr-ABT}$ ) MNPs)

$\text{MnCoFe}_2\text{O}_4\text{@SiO}_2\text{-Pr-Cl}$  MNPs (0.5 g) were dispersed in DMF (20 mL) under ultrasound waves for 20 min. 2-Aminobenzothiazole (ABT) (2 mmol, 0.3 g) and trimethylamine (2 mmol, 0.3 mL) were added and the mixture refluxed for 48 h. The obtained preparation was then filtered by an external magnetic field, washed with DMF until it became colorless and dried in an oven at 70  $^\circ\text{C}$ .

#### 2.1.5. Preparation of Zn complexed on MCF MNPs (MCF@ $\text{SiO}_2\text{-Pr-ABT@ZnCl}_2$ MNPs)

MCF@ $\text{SiO}_2\text{-Pr-ABT}$  nanoparticles (0.5 g) were exposed to ultrasound in ethanol (99 %, 20 mL) for 20 min,  $\text{ZnCl}_2\cdot 4\text{H}_2\text{O}$  (2 mmol, 0.42 g) was added and refluxed for 24 h. MCF@ $\text{SiO}_2\text{-Pr-ABT@ZnCl}_2$  MNPs were isolated by a magnet and washed with 20 mL ethanol and dried in oven at 70  $^\circ\text{C}$ .



**Scheme 1.** The synthetic steps of MCF@SiO<sub>2</sub>-Pr-ABT@ZnCl<sub>2</sub> MNPs.

#### 2.1.6. Preparation of 2-amino-4H-pyran and N-arylquinoline derivatives

To a well stirred mixture of aromatic aldehyde (1 mmol) (1), malononitrile (2) (1 mmol), and  $\beta$ -ketoester (4-hydroxycumarin (3) or barbituric acid (4) or dimedone (5) or 5,5-dimethyl-3-(phenylamino)cyclohex-2-en-1-one (6) (1 mmol)) in EtOH:H<sub>2</sub>O (1:1) were added MCF@SiO<sub>2</sub>-Pr-ABT@ZnCl<sub>2</sub> MNPs (15 mg). The mixture was refluxed and the progress of the reaction controlled by TLC. The solvent was evaporated and the mixture diluted with 10 mL of ethanol so that the catalyst could be well separated by magnet. The isolated catalyst was washed several time with EtOH, dried in oven and reused in next reaction. Then, the solution was cooled at room temperature to give crystals of 2-amino-4H-pyran and N-arylquinoline derivatives.

#### 2.1.7. Selected data

**2-Amino-4-(4-chlorophenyl)-5-oxo-4H,5H-pyrano [3,2-c]chromene-3-carbonitrile (7b):** IR (KBr) ( $\nu_{\max}$ , cm<sup>-1</sup>): 3373, 3323, 3168, 2979, 2933, 2212, 1725, 1658, 1591, 1282, 763. <sup>1</sup>H NMR (300 MHz, DMSO-*d*<sub>6</sub>):  $\delta_{\text{H}}$  = 4.59 (s, 1H, CH), 7.62–7.45 (m, 6H, H<sub>Ar</sub>, NH<sub>2</sub>), 7.80–7.69 (m, 4H, H<sub>Ar</sub>) ppm.

**2-Amino-4-(4-nitrophenyl)-5-oxo-4H,5H-pyrano [3,2-c]chromene-3-carbonitrile (7c):** IR (KBr) ( $\nu_{\max}$ , cm<sup>-1</sup>): 3398, 3323, 3189, 3088, 2195, 1700, 1675, 1530, 1379. <sup>1</sup>H NMR (300 MHz, DMSO-*d*<sub>6</sub>):  $\delta_{\text{H}}$  = 4.67 (s, 1H, CH), 7.45–7.60 (m, 4H, H<sub>Ar</sub>), 7.53 (s, 2H, NH<sub>2</sub>), 7.89–7.92 (d, *J* = 8.0 Hz, 2H, H<sub>Ar</sub>), 8.16–8.18 (d, *J* = 8.0 Hz, 2H, H<sub>Ar</sub>) ppm.

**2'-Amino-2,5'-dioxo-5'H-spiro[indoline-3,4'-pyrano [3,2-c]chromene]-3'-carbonitrile: (7h)** IR (KBr) ( $\nu_{\max}$ , cm<sup>-1</sup>): 3358, 3308, 3199, 2204, 1730, 1672, 1609, 1474, 1359. <sup>1</sup>H NMR (300 MHz, DMSO-*d*<sub>6</sub>):  $\delta_{\text{H}}$  = 6.91 (d, *J* = 8.0 Hz, 1H, H<sub>Ar</sub>), 6.98 (d, *J* = 7.0 Hz, 1H, H<sub>Ar</sub>), 7.29–7.24 (m, 3H, H<sub>Ar</sub>), 7.62–7.47 (m, 3H, H<sub>Ar</sub>), 7.78 (s, 2H, NH<sub>2</sub>), 8.02 (d, *J* = 8.0 Hz, 1H, H<sub>Ar</sub>), 10.79 (s, 1H, NH).

**7-Amino-2,4-dioxo-5-phenyl-1,3,4,5-tetrahydro-2H-pyrano [2,3-d]pyrimidine-6-carbonitrile (8a):** IR (KBr) ( $\nu_{\max}$ , cm<sup>-1</sup>): 3385, 3305, 3183, 3073, 2838, 2195, 1720, 1676, 1637, 1601, 1522, 1278. <sup>1</sup>H NMR (300 MHz, DMSO-*d*<sub>6</sub>):  $\delta_{\text{H}}$  = 4.20 (s, 1H, CH), 7.12–7.26 (m, 7H, H<sub>Ar</sub> and NH<sub>2</sub>), 11.07 (s, 1H, NH), 12.08 (s, 1H, NH) ppm.

**7-Amino-5-(4-chlorophenyl)-2,4-dioxo-1,3,4,5-tetrahydro-2H-pyrano [2,3-d]pyrimidine-6-carbonitrile (8b):** IR (KBr) ( $\nu_{\max}$ , cm<sup>-1</sup>): 3391, 3306, 3214, 3089, 2953, 2196, 1717, 1676, 1638, 1584, 1489, 1281, 828. <sup>1</sup>H NMR (300 MHz, DMSO-*d*<sub>6</sub>):  $\delta_{\text{H}}$  = 4.23 (s, 1H, CH), 7.26 (d, *J* = 7.0 Hz, 2H, H<sub>Ar</sub>), 7.72 (d, *J* = 7.0 Hz, 2H, H<sub>Ar</sub>), 8.55 (s, 2H, NH<sub>2</sub>), 11.14 (s, 1H, NH), 11.68 (s, 1H, NH) ppm.

**2-Amino-4-(3-hydroxyphenyl)-7,7-dimethyl-5-oxo-5,6,7,8-tetrahydro-4H-chromene-3-carbonitrile (9c):** IR (KBr) ( $\nu_{\max}$ , cm<sup>-1</sup>): 3456, 3314, 2965, 2198, 1680, 1642, 1595, 1481, 1215. <sup>1</sup>H NMR (300 MHz, DMSO-*d*<sub>6</sub>):  $\delta_{\text{H}}$  = 0.95 (s, 3H, CH<sub>3</sub>), 1.03 (s, 3H, CH<sub>3</sub>), 2.10 (d, *J* = 16.0 Hz, 1H, CH), 2.25 (d, *J* = 17.0 Hz, 1H, CH), 2.45 (d, *J* = 17.0 Hz, 2H, CH<sub>2</sub>), 4.06 (s, 1H, CH), 6.53–7.05 (m, 6H, H<sub>Ar</sub> & NH<sub>2</sub>), 8.90 (s, 1H, OH) ppm.

**4,4'-(1,4-Phenylene)bis(2-amino-7,7-dimethyl-5-oxo-5,6,7,8-tetrahydro-4H-chromene-3-carbonitrile) (9f):** IR (KBr) ( $\nu_{\max}$ , cm<sup>-1</sup>): 3452, 3332, 3174, 2960, 2194, 1665, 1598, 1213. <sup>1</sup>H NMR (300 MHz, DMSO-*d*<sub>6</sub>):  $\delta_{\text{H}}$  = 0.92–1.02) m, 12H, 4CH<sub>3</sub>), 1.90–2.22 (m, 8H, 4CH<sub>2</sub>), 4.12 (s, 2H, 2CH), 7.00 (d, *J* = 10.1 Hz, 8H, H<sub>Ar</sub> & NH<sub>2</sub>) ppm.

**2-Amino-7,7-dimethyl-5-oxo-1-phenyl-4-(p-tolyl)-1,4,5,6,7,8-hexahydroquinoline-3-carbonitrile (10d):** IR (KBr) ( $\nu_{\max}$ , cm<sup>-1</sup>): 3458, 3333, 3217, 2956, 2926, 2178, 1654. <sup>1</sup>H NMR (300 MHz, DMSO-*d*<sub>6</sub>):  $\delta_{\text{H}}$  = 1.00 (s, 3H, CH<sub>3</sub>), 1.14 (s, 3H, CH<sub>3</sub>), 1.94 (d, *J* = 10.5 Hz, 1H, CH), 2.26 (d, *J* = 14.7 Hz, 1H, CH), 2.43 (s, 2H, CH<sub>2</sub>), 2.77 (s, 3H, CH<sub>3</sub>), 4.69 (s, 1H, CH), 5.60 (s, 2H, NH<sub>2</sub>), 7.42–7.86 (m, 9H,

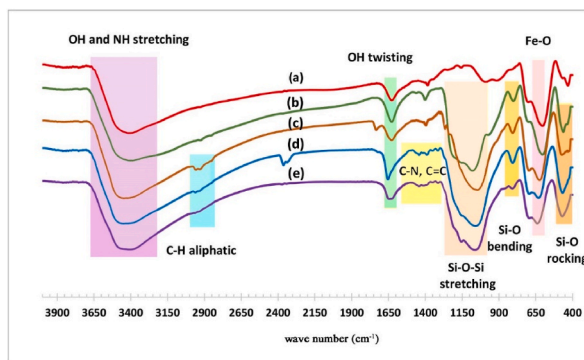


**Fig. 1.** FT-IR spectra of MnCoFe<sub>2</sub>O<sub>4</sub> (MCF) (a), silica-coated MCF MNPs (MCF@SiO<sub>2</sub>) (b), Functionalized MCF@SiO<sub>2</sub> by CPTS (MCF@SiO<sub>2</sub>-Pr-Cl) (c), Modification of MnCoFe<sub>2</sub>O<sub>4</sub>@SiO<sub>2</sub>-Pr-Cl by 2-aminobenzothiazole (MCF@SiO<sub>2</sub>-Pr-ABT) (d) and Zn complexed on MCF MNPs (MCF@SiO<sub>2</sub>-Pr-ABT@ZnCl<sub>2</sub>) (e) MNPs in range of 400–4000 cm<sup>-1</sup>.

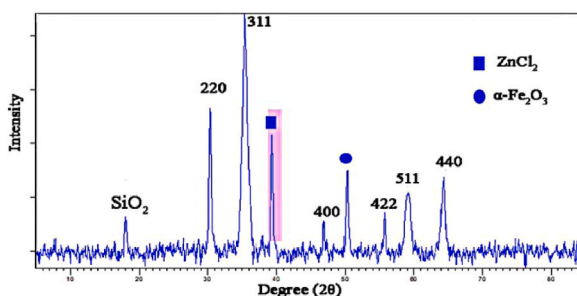


**Fig. 2.** XRD pattern of MCF@SiO<sub>2</sub>-Pr-ABT@ZnCl<sub>2</sub> MNPs.

H<sub>Ar</sub>) ppm.

**2-Amino-4-(4-hydroxy-3-nitrophenyl)-7,7-dimethyl-5-oxo-1-phenyl-1,4,5,6,7,8-hexahydroquinoline-3-carbonitrile (10e):** IR (KBr) ( $\nu_{\max}$ , cm<sup>-1</sup>): 3464, 3324, 3215, 2958, 2890, 2179, 1652. <sup>1</sup>H NMR (300 MHz, DMSO-*d*<sub>6</sub>):  $\delta_{\text{H}}$  = 0.99 (s, 3H, CH<sub>3</sub>), 1.16 (s, 3H, CH<sub>3</sub>), 1.96 (d, *J* = 17.4 Hz, 1H, CH<sub>2</sub>), 2.27 (d, *J* = 15.1 Hz, 1H, CH<sub>2</sub>), 2.46 (s, 2H, CH<sub>2</sub>), 4.75 (s, 1H, CH), 5.76 (s, 2H, NH<sub>2</sub>), 7.42–8.01 (m, 8H, H<sub>Ar</sub>), 10.12 (brs, 1H, OH) ppm.

**2-Amino-4-(4-(2-amino-3-cyano-6,6-dimethyl-8-oxo-4-phenyl-1,4,5,6,7,8-hexahydronaphthalen-1-yl)phenyl)-7,7-dimethyl-5-oxo-1-phenyl-1,4,5,6,7,8-hexahydroquinoline-3-carbonitrile (10f):** IR (KBr) ( $\nu_{\max}$ , cm<sup>-1</sup>): 3468, 3236, 3061, 2957, 2181, 1644. <sup>1</sup>H NMR (300 MHz, DMSO-*d*<sub>6</sub>):  $\delta_{\text{H}}$  = 0.74 (s, 3H, CH<sub>3</sub>), 0.88 (s, 3H, CH<sub>3</sub>), 1.02 (s, 6H, 2CH<sub>3</sub>), 1.74 (d, *J* = 16.0 Hz, 2H, CH<sub>2</sub>), 2.04 (s, 2H), 2.16 (d, *J* = 16.0 Hz, 2H, CH<sub>2</sub>), 2.38 (s, 2H, CH<sub>2</sub>), 4.48 (s, 2H, 2CH), 5.4 (s, 4H, 2NH<sub>2</sub>), 7.16–7.57 (m, 14H, H<sub>Ar</sub>).

### 3. Results and discussion

The synthetic steps of MCF@SiO<sub>2</sub>-Pr-ABT@ZnCl<sub>2</sub> MNPs are presented in [Scheme 1](#). MCF MNPs were prepared by the co-precipitation method (Mn<sup>+2</sup>:Co<sup>+2</sup>:Fe<sup>+3</sup> with a molar ratio (1:1:4) and under basic condition) [28]. These nanoparticles were coated with silica (MCF@SiO<sub>2</sub> MNPs) using Stöber method [29]. Then, surface of MCF@SiO<sub>2</sub> MNPs was functionalized by the CPTS and 2-ABT [30]. Finally, ZnCl<sub>2</sub> was loaded on the surface of MCF@SiO<sub>2</sub>-Pr-ABT MNPs to prepare MCF@SiO<sub>2</sub>-Pr-ABT@ZnCl<sub>2</sub> MNPs.

Characterization of MCF@SiO<sub>2</sub>-Pr-ABT@ZnCl<sub>2</sub> MNPs was carried out by techniques such as FT-IR, FE-SEM, EDS, XRD, ICP, TGA, and VSM.

#### 3.1. FT-IR spectra

FT-IR spectra of MCF (a), MCF@SiO<sub>2</sub> (b), MCF@SiO<sub>2</sub>-Pr-Cl (c), MCF@SiO<sub>2</sub>-Pr-ABT (d) and MCF@SiO<sub>2</sub>-Pr-ABT@ZnCl<sub>2</sub> (e) MNPs are presented in [Fig. 1](#). The appeared adsorption bands at 3412–3423 cm<sup>-1</sup> and 1627–1645 cm<sup>-1</sup> are due to OH stretching and OH twisting, respectively ([Fig. 1a–e](#)). The observed bands at 602–630 cm<sup>-1</sup> can prove the presence of Fe–O stretching vibrations ([Fig. 1a–e](#)). The presence of Si–O–Si stretching, Si–O bending, and Si–O rocking verify by the adsorption bands at (1080–1063 cm<sup>-1</sup>), [(973 cm<sup>-1</sup>), (801–808 cm<sup>-1</sup>)], and (461–467 cm<sup>-1</sup>), respectively ([Fig. 1b–e](#)). The observed weak bands at 2957 and 2931 cm<sup>-1</sup> confirm the presence of C–H aliphatic of CPTS in the structure of the nanocatalyst ([Fig. 1c–e](#)). The adsorption band at 1653 cm<sup>-1</sup> in [Fig. 1d](#) is belong to N–H bending of ABT in the structure of nanoparticles. In addition, the vibrations of C–N and C]C groups are observed at 1441 and 1388 cm<sup>-1</sup>, respectively ([Fig. 1d](#)). The vibration frequency shifts from 1653 cm<sup>-1</sup> ([Fig. 1d](#)) to 1645 cm<sup>-1</sup>

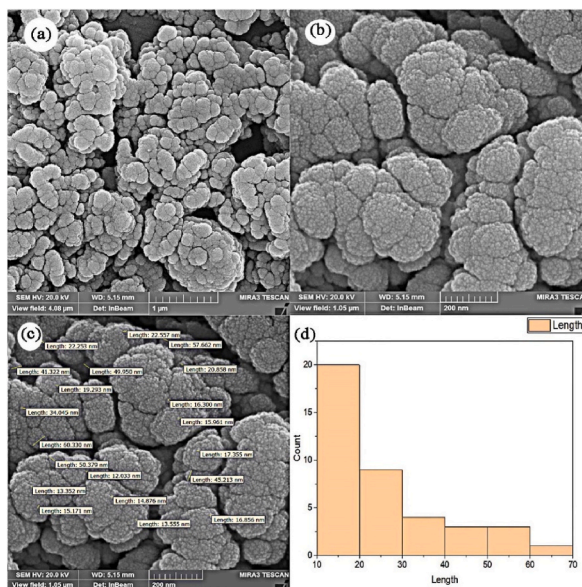


Fig. 3. FE-SEM images of MCF@SiO<sub>2</sub>-Pr-ABT@ZnCl<sub>2</sub> MNPs.

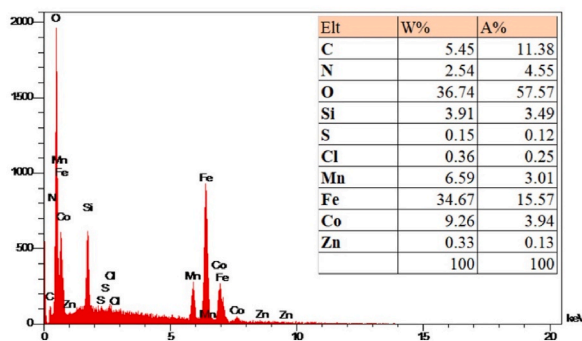


Fig. 4. EDX analysis of MCF@SiO<sub>2</sub>-Pr-ABT@ZnCl<sub>2</sub> MNPs.

(Fig. 1e) can be attributed to the successful immobilization of ZnCl<sub>2</sub> on MNPs. Also, the changing vibration frequency for Fe–O, Si–O–Si, and Si–O adsorption bands is due to the interaction between MCF and TEOS, TEOS with CPTS, and CPTS with ABT.

### 3.2. XRD pattern

The XRD pattern of MCF@SiO<sub>2</sub>-Pr-ABT@ZnCl<sub>2</sub> MNPs (Fig. 2) shows a peak at about  $2\theta = 18^\circ$ , which confirms the loading of the amorphous SiO<sub>2</sub> layer onto the surface of MCF MNPs. Also, the loading of ZnCl<sub>2</sub> onto the surface of MCF@SiO<sub>2</sub>-Pr-ABT MNPs can be verified by the diffraction peaks at  $2\theta = 39^\circ$  [31]. The presence of peaks at  $2\theta = 32^\circ, 35^\circ, 42^\circ, 52^\circ, 59^\circ$  and  $63^\circ$  is in support of crystalline structure of the MCF MNPs, which is according to JCPDS No. 22–1086 standard reported by Datt and colleagues [32]. Also, the presence of a peak at  $2\theta = 50^\circ$  confirms  $\alpha$ -Fe<sub>2</sub>O<sub>3</sub> MNPs in the structure [33]. The crystal size of MNPs was calculated to be about 23 nm by Scherrer's equation. The crystal size is according to the value obtained by the FE-SEM analysis data.

### 3.3. FE-SEM analysis

FE-SEM technique was utilized to evaluate the size and the morphology of MCF@SiO<sub>2</sub>-Pr-ABT@ZnCl<sub>2</sub> MNPs (Fig. 3). The images confirm the uniform cauliflower structure with uneven surfaces, which increases the surface-to-volume ratio and improves the catalytic activity of nanoparticles [7]. Also, the FE-SEM images (Fig. 3a–c) show different size distributions of NPs, which can confirm the aggregation in MNP structures. The histogram chart (Fig. 3d) shows an average size of in the range 10–20 nm for NPs.



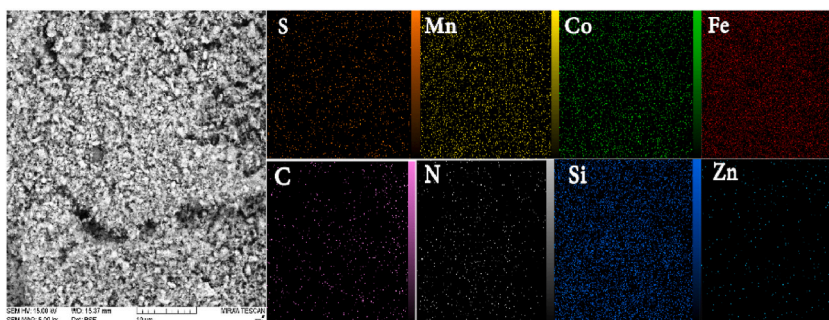


Fig. 5. Mapping analysis of MCF@SiO<sub>2</sub>-Pr-ABT@ZnCl<sub>2</sub> MNPs.

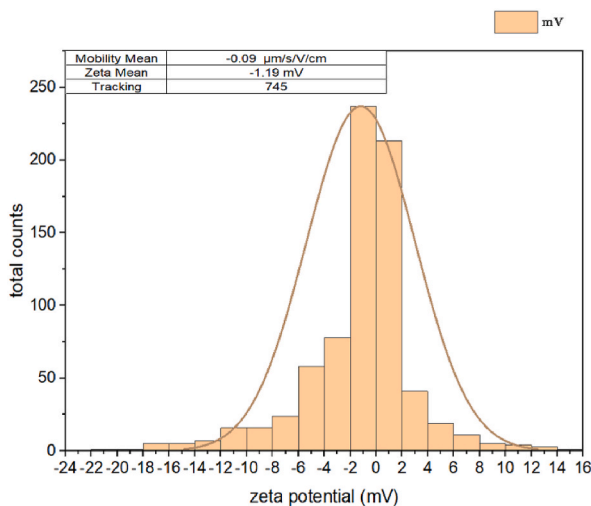


Fig. 6. Zeta potential analysis of MCF@SiO<sub>2</sub>-Pr-ABT@ZnCl<sub>2</sub> MNPs.

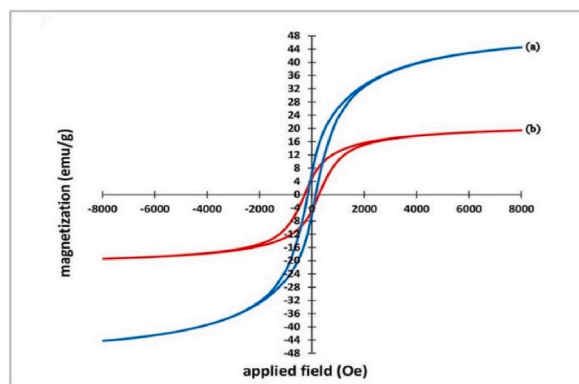
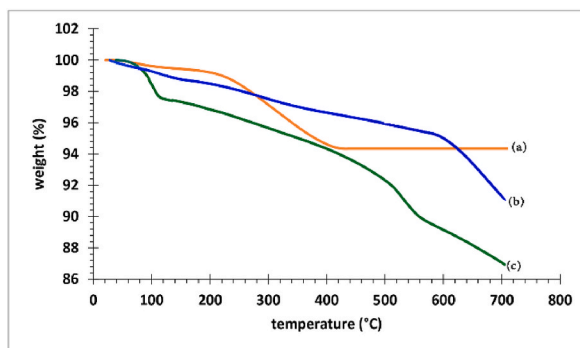


Fig. 7. VSM analysis of MCF@SiO<sub>2</sub>-Pr-ABT@ZnCl<sub>2</sub> MNPs.

### 3.4. EDX and mapping analyses

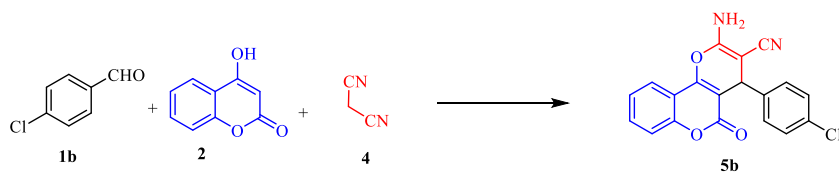
EDX analysis of MCF@SiO<sub>2</sub>-Pr-ABT@ZnCl<sub>2</sub> MNPs is displayed in Fig. 4. The EDX spectrum of MCF@SiO<sub>2</sub>-Pr-ABT@ZnCl<sub>2</sub> MNPs and related data show the presence of Mn, Co, Fe, Si, O, C, Cl, N, S and Zn elements. The presence of Cl element in structure MNPs can be for two reasons. One of the reasons is that the modification of the nanoparticle surface has not occurred completely and only parts of the nanoparticle surface, not the whole, are modified by ABT. Another important reason is the loading of zinc chloride on the surface of nanoparticles. Fig. 5 was utilized for mapping analysis to validate the findings of EDX analysis. Furthermore, the results of ICP analysis



**Fig. 8.** The investigation of thermal stability of MnCoFe<sub>2</sub>O<sub>4</sub> (MCF) (a), functionalized MCF@SiO<sub>2</sub> by CPTS (MCF@SiO<sub>2</sub>-Pr-Cl) (b), and Zn complexed on MCF MNPs (MCF@SiO<sub>2</sub>-Pr-ABT@ZnCl<sub>2</sub>) (c) MNPs by TGA analysis at 25 °C–700 °C.

**Table 1**

Optimization of reaction conditions for the synthesis of 2-amino-4H-pyran in the presence of MCF@SiO<sub>2</sub>-Pr-ABT@ZnCl<sub>2</sub>



Entry	Catalyst (mg)	Solvent	Temperature (°C)	Time (h)	Yield <sup>a</sup> (%)
1	MCF@SiO <sub>2</sub> -Pr-ABT@ZnCl <sub>2</sub> (10)	H <sub>2</sub> O	75	5 h	70
2	MCF@SiO <sub>2</sub> -Pr-ABT@ZnCl <sub>2</sub> (10)	EtOH:H <sub>2</sub> O(1:1)	75	2	85
3	MCF@SiO <sub>2</sub> -Pr-ABT@ZnCl <sub>2</sub> (10)	EtOH	75	4.20	72
4	MCF@SiO <sub>2</sub> -Pr-ABT@ZnCl <sub>2</sub> (10)	DMF	75	8	Trace
5	MCF@SiO <sub>2</sub> -Pr-ABT@ZnCl <sub>2</sub> (10)	CH <sub>3</sub> CN	reflux	8	Trace
6	MCF@SiO <sub>2</sub> -Pr-ABT@ZnCl <sub>2</sub> (10)	Solvent free	75	4.50	73
7	–	EtOH:H <sub>2</sub> O(1:1)	75	24	Trace
8	MCF@SiO <sub>2</sub> -Pr-ABT@ZnCl <sub>2</sub> (5)	EtOH:H <sub>2</sub> O(1:1)	75	3.25	80
9	MCF@SiO <sub>2</sub> -Pr-ABT@ZnCl <sub>2</sub> (15)	EtOH:H <sub>2</sub> O(1:1)	75	1	93
10	MCF@SiO <sub>2</sub> -Pr-ABT@ZnCl <sub>2</sub> (18)	EtOH:H <sub>2</sub> O(1:1)	75	1	93
11	MCF@SiO <sub>2</sub> -Pr-ABT@ZnCl <sub>2</sub> (15)	EtOH:H <sub>2</sub> O(1:1)	r.t	12	60
12	MCF@SiO <sub>2</sub> -Pr-ABT@ZnCl <sub>2</sub> (15)	EtOH:H <sub>2</sub> O(1:1)	50	3.55	70
13	MCF (15)	EtOH:H <sub>2</sub> O(1:1)	75	2.10	80
14	MCF@SiO <sub>2</sub> -Pr-ABT (15)	EtOH:H <sub>2</sub> O(1:1)	75	3.15	80

<sup>a</sup> Isolated yield. condition: 4-hydroxycoumarin (1 mmol, 0.16 g), 4-chloro benzaldehyde (1 mmol, 0.14 g) and malononitrile (1 mmol, 0.06 g).

show that 0.13 mmol/g Zn is loaded on the surface of MNPs.

### 3.5. The zeta potential analysis

The zeta potential analysis showed that the surface charge of MCF@SiO<sub>2</sub>-Pr-ABT@ZnCl<sub>2</sub> MNPs was negative (Zeta mean: –1.19 mV) (Fig. 6). The low value of the zeta potential of MNPs confirms a poor stability for MNPs in aqueous solutions. The low zeta potential values improve van der Waals interparticle attractions and lead to the aggregation of NPs [34]. The FE-SEM images can confirm the aggregation in the MNP structures and are consistent with the zeta potential analysis. This poor stability can be a result of the steric hindrance of alkyl silanes. Alkyl silanes can prevent proton diffusion to the MNPs by creating a strong hydrophobic layer and produce the lower zeta potential of MNPs. Therefore, the zeta potential of the MNPs can be decreased after coating with compounds such as alkyl silanes [35,36].

### 3.6. VSM analysis

The VSM analysis was obtained for MCF (a), and MCF@SiO<sub>2</sub>-Pr-ABT@ZnCl<sub>2</sub> MNPs (b) at room temperature in the range of ±8000 Oe (Fig. 7) to investigate the effect of modification on magnetic properties of MCF@SiO<sub>2</sub>-Pr-ABT@ZnCl<sub>2</sub> MNPs. The hysteresis loops indicate a decreasing of the magnetization saturation value (M<sub>s</sub>) from 44 (MCF) to 20 (MCF@SiO<sub>2</sub>-Pr-ABT@ZnCl<sub>2</sub>) emu<sup>-1</sup>. This demagnetization (M<sub>s</sub>) is caused by larger particles, which happens when organic coatings are added to the magnetic nanoparticles

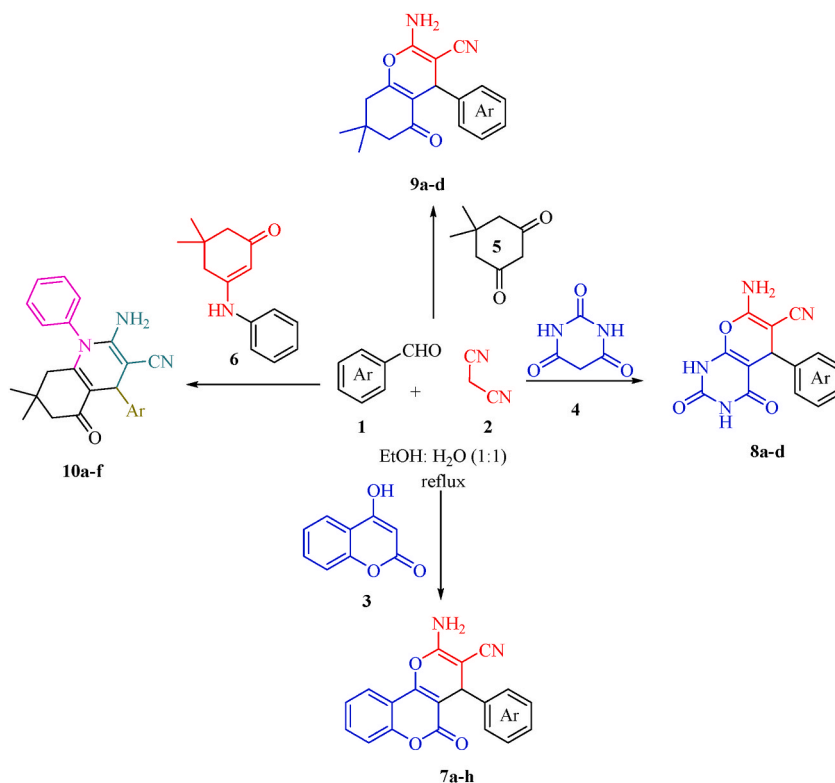
**Table 2**

The synthesis of 2-amino-4*H*-pyran and *N*-arylquinoline derivatives in the presence of MCF@SiO<sub>2</sub>-Pr-ABT@ZnCl<sub>2</sub> catalyst under optimized conditions.

Entry	Ar or carbonyl group	1,3-dicarbonyl	product	Time (min)	Yield (%)	Mp (°C)		Ref
						found	Reported	
1	C <sub>6</sub> H <sub>5</sub> CHO	3	7a	45	93	255–258	257–258	[39]
2	4-ClC <sub>6</sub> H <sub>4</sub> CHO	3	7b	40	92	247–250	249–251	[40]
3	4-NO <sub>2</sub> C <sub>6</sub> H <sub>4</sub> CHO	3	7c	40	87	249–252	256–257	[39]
4	3-NO <sub>2</sub> C <sub>6</sub> H <sub>4</sub> CHO	3	7d	55	80	257–258	257–259	[40]
5	2,4-Cl <sub>2</sub> C <sub>6</sub> H <sub>3</sub> CHO	3	7e	56	84	247–249	253–255	[40]
6	3-OHC <sub>6</sub> H <sub>4</sub> CHO	3	7f	65	80	240–243	248–250	[41]
7	4-OHC <sub>6</sub> H <sub>4</sub> CHO	3	7g	76	81	270–272	263–265	[40]
8	Isatin	3	7h	70	82	257–263	280–282	[42]
9	C <sub>6</sub> H <sub>5</sub> CHO	4	8a	48	93	201–202	206–208	[43]
10	4-ClC <sub>6</sub> H <sub>4</sub> CHO	4	8b	48	92	227–228	223–225	[43]
11	4-OHC <sub>6</sub> H <sub>4</sub> CHO	4	8c	75	82	270–271	278–280	[44]
12	Isatin	4	8d	68	82	278–280	280–282	[42]
13	C <sub>6</sub> H <sub>5</sub> CHO	5	9a	25	90	235–236	236–238	[45]
14	4-ClC <sub>6</sub> H <sub>4</sub> CHO	5	9b	20	95	210–212	215–216	[11]
15	3-OHC <sub>6</sub> H <sub>4</sub> CHO	5	9c	23	83	235–238	236–237	[28]
16	Terphthalaldehydet <sup>a</sup>	5	9f	45	86	263–264	266–269	[28]
17	4-Cl-C <sub>7</sub> H <sub>5</sub> O	6	10a	25	90	268–270	268–269	[46]
18	4-CH <sub>3</sub> -C <sub>7</sub> H <sub>5</sub> O	6	10d	55	91	240–241	244–245	[11]
19	4-OH,3-NO <sub>2</sub> -C <sub>7</sub> H <sub>4</sub> O	6	10e	25	90	271–272	272–274	[27]
20	Terphthalaldehyde <sup>b</sup>	6	10f	50	83	233–236	237–238	[27]

<sup>a</sup> Isolated yields, Aromatic aldehyde (1 mmol) (1), malononitrile (2) (1 mmol), and β-ketoester (4-hydroxycumarin (3) or barbituric acid (4) or dimedone (5) or 5,5-dimethyl-3-(phenylamino)cyclohex-2-en-1-one (6) (1 mmol)) in the presence of MCF@SiO<sub>2</sub>-Pr-ABT@ZnCl<sub>2</sub> (15 mg) as catalyst, EtOH:H<sub>2</sub>O (5 mL) under reflux conditions.

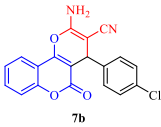
<sup>b</sup> Aromatic aldehyde (0.5 mmol) (1), malononitrile (2) (1 mmol), and β-ketoester (4-hydroxycumarin (3) or barbituric acid (4) or dimedone (5) or 5,5-dimethyl-3-(phenylamino)cyclohex-2-en-1-one (6) (1 mmol)) in the presence of MCF@SiO<sub>2</sub>-Pr-ABT@ZnCl<sub>2</sub> (15 mg) as catalyst, EtOH:H<sub>2</sub>O (5 mL) under reflux conditions.

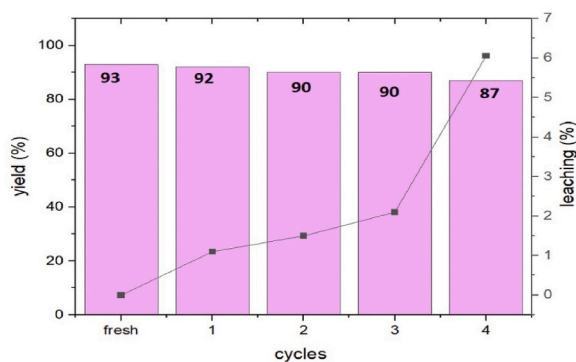


**Scheme 2.** The synthesis of 2-amino-4*H*-pyrans under optimal conditions.



**Table 3**Comparison of the catalytic activity of MCF@SiO<sub>2</sub>-Pr-ABT@ZnCl<sub>2</sub> and other known catalysts for model reaction (synthesis of **7b**).

Compound	Entry	Catalyst	Conditions	Time (min)	Yield (%)	Ref.
 7b	1	Fe <sub>3</sub> O <sub>4</sub> @SiO <sub>2</sub> @BenzIm-Fc[Cl]/NiCl <sub>2</sub> nanocatalyst	EtOH:H <sub>2</sub> O (4:2), r.t	15	95	[7]
	2	polyaniline/SiO <sub>2</sub>	EtOH:H <sub>2</sub> O (1:1), reflux	15	90	[47]
	3	β-CD	H <sub>2</sub> O, 60–65 °C	120	72	[48]
	4	Ca <sub>9.5</sub> Mg <sub>0.5</sub> (PO <sub>4</sub> ) <sub>5.5</sub> (SiO <sub>4</sub> ) <sub>0.5</sub> F <sub>1.5</sub>	EtOH:H <sub>2</sub> O (1:1), reflux	60	90	[39]
	5	Sodium Dodecyl Sulfate	H <sub>2</sub> O, reflux	180	88	[49]
	6	MgO nanoplates	H <sub>2</sub> O, reflux	120	84	[50]
	7	<b>MCF@SiO<sub>2</sub>-Pr-ABT@ZnCl<sub>2</sub></b>	<b>EtOH:H<sub>2</sub>O (1:1), 75 °C</b>	<b>40</b>	<b>92</b>	<b>This work</b>

**Fig. 9.** Reusability and recyclability of the MCF@SiO<sub>2</sub>-Pr-ABT@ZnCl<sub>2</sub> MNPs during four runs.

[37].

### 3.7. TGA analysis

The weight loss of MCF (a), MCF@SiO<sub>2</sub>-Pr-Cl (b), and MCF@SiO<sub>2</sub>-Pr-ABT@ZnCl<sub>2</sub> (c) was studied using TGA analysis by increasing the reaction temperature from room temperature to 700 °C (Fig. 8). The TGA analyses of MCF (a), MCF@SiO<sub>2</sub>-Pr-Cl (b), and MCF@SiO<sub>2</sub>-Pr-ABT@ZnCl<sub>2</sub> (c) MNPs showed 5.5 %, 8.8 %, and 13 % weight loss, respectively. The first step of TGA analyses for three samples show a weight loss for MNPs at T < 110 °C (0.4 % weight loss for MCF, 1.2 % weight loss for MCF@SiO<sub>2</sub>-Pr-Cl, and 2 % weight loss for MCF@SiO<sub>2</sub>-Pr-ABT@ZnCl<sub>2</sub>). In the first stage of diagram, the weight loss in three samples is due to the removal of water and organic solvents from the surface of MNPs. In the second step for MCF (Fig. 8a), and for MCF@SiO<sub>2</sub>-Pr-Cl (Fig. 8b) the weight losses are about 5.1 % (at 110 °C < T < 400 °C) and 4.2 % (at 110 °C < T < 600 °C, respectively). The weight loss about 4.1 % of MCF@SiO<sub>2</sub>-Pr-Cl is corresponded to the decomposition of the organic layer in MCF@SiO<sub>2</sub>-Pr-Cl (Fig. 8b). The 5.1 % weight loss of MCF can be related to disruption of the MNPs structure (Fig. 8a). Also, In the second step for MCF@SiO<sub>2</sub>-Pr-ABT@ZnCl<sub>2</sub> (Fig. 8c), the observed weight loss of about 7.5 % in the range of 110 °C < T < 575 °C is corresponded to the decomposition of the organic layer in the MNPs. These results support the synthesis of MCF@SiO<sub>2</sub>-Pr-ABT@ZnCl<sub>2</sub> MNPs.

### 3.8. The catalytic activity of MCF@SiO<sub>2</sub>-Pr-ABT@ZnCl<sub>2</sub> MNPs for the synthesis of 2-amino-4H-pyran and N- arylquinoline derivatives

The catalytic activity of MCF@SiO<sub>2</sub>-Pr-ABT@ZnCl<sub>2</sub> MNPs was investigated for the synthesis of 2-amino-4H-pyran and N- arylquinoline derivatives. For this purpose, the reaction of 4-hydroxycoumarin (1 mmol), malononitrile (1.1 mmol), and 4-chloro benzaldehyde was selected as a model reaction and investigated by considering parameters including type of solvent, temperatures, and amount of catalysts (Table 1). The highest yield of product (93 %) was achieved in EtOH:H<sub>2</sub>O (1:1) as a solvent, 15 mg of catalyst under reflux condition (Table 1, Entry 9). Also for comparison, the catalytic activity of MCF, MCF@SiO<sub>2</sub>-Pr-ABT and MCF@SiO<sub>2</sub>-Pr-ABT@ZnCl<sub>2</sub> MNPs was investigated under optimal condition. MCF@SiO<sub>2</sub>-Pr-ABT@ZnCl<sub>2</sub> MNPs provided a more favorable result (Table 1, Entry 13, and 14) and confirms that ZnCl<sub>2</sub> has an essential role in the reaction progress. Also, MnCoFe<sub>2</sub>O<sub>4</sub> nanoparticles were chosen as the catalyst base due to their chemical stability and having two active sites of cobalt and manganese [38]. Under the optimized reaction conditions, the protocol was evaluated for the synthesis of different 2-amino-4H-pyrans and N- arylquinolines by using different types of aldehydes, malononitrile, and ethyl acetate. The results are summarized Table 2 and Scheme 2. As the findings show, this process is possible for the synthesis of desired compounds using aromatic aldehydes, with both electron-donating and electron-withdrawing groups, with high efficiency. Also, the results of this research were compared with those reported in the literature for model reaction (Table 3).

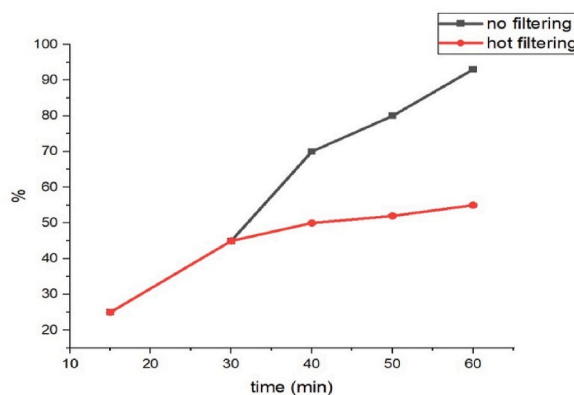


**Fig. 10.** Hot filtration test for the MCF@SiO<sub>2</sub>-Pr-ABT@ZnCl<sub>2</sub> MNPs catalyzed the model reaction (t = 40 min).

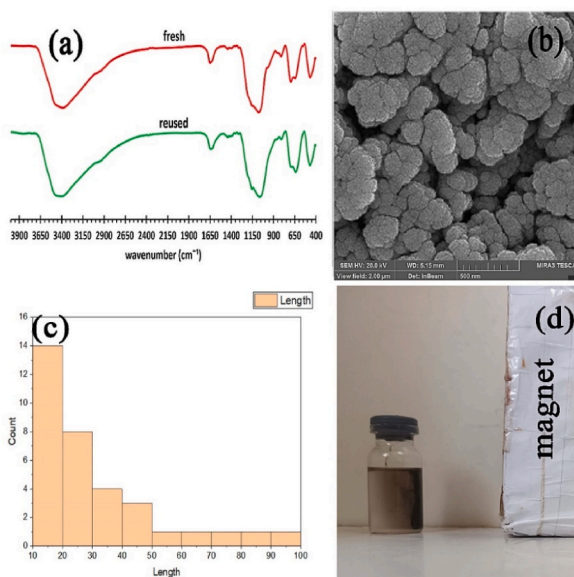


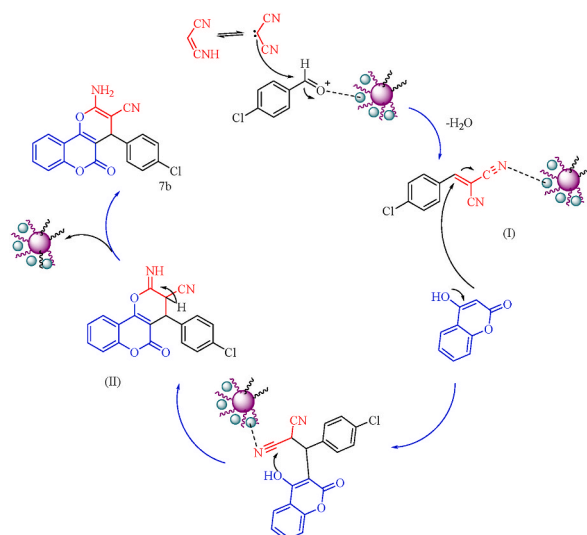
**Fig. 11.** FT-IR spectra (a) for fresh and reused catalyst (after five runs) (which is mentioned in the figure of spectra), FE-SEM image (b), histogram chart (c) and magnetic property (d) for reused catalyst after five runs.

### 3.9. Reusability and recyclability of the MCF@SiO<sub>2</sub>-Pr-ABT@ZnCl<sub>2</sub> MNPs

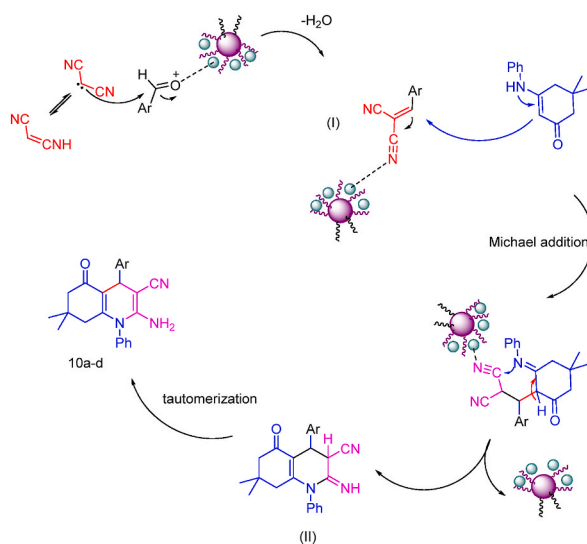
The reusability of MCF@SiO<sub>2</sub>-Pr-ABT@ZnCl<sub>2</sub> MNPs was investigated for **7b** compound. After completion of the reaction, the catalyst was isolated by a magnet, washed with EtOH several times, and reused for the synthesis of **7b**. Using the catalyst after five runs shows that the effectiveness of MCF@SiO<sub>2</sub>-Pr-ABT@ZnCl<sub>2</sub> MNPs has decreased slightly. Also, the leaching rate of zinc from the MCF@SiO<sub>2</sub>-Pr-ABT@ZnCl<sub>2</sub> nanoparticles was quantified through ICP analysis after each cycle. It was observed that only 6 % Zn leached after the fifth runs. These findings showed a little change in the percentage of Zn into the organic solution and the heterogeneous nature of the system, which confirms the stability of the framework under reaction conditions (Fig. 9).

The hot filtration test was performed during the model reaction under optimal conditions. The reaction was refluxed to achieve 50 % yield within 20 min. MNPs were then rapidly separated from the reaction mixture by a magnet, followed by stirring for another 20 min. After removing the catalyst, no increase was observed in reaction yield, confirming the absence of any catalyst in the filter (Fig. 10).

Structure of fresh and reused catalyst were compared by the FT-IR spectra (Fig. 11a), FE-SEM analysis (Fig. 11b), and histogram chart (Fig. 11c). This comparison confirmed that the structure of catalyst is preserved during five runs. The amount of Zn leaching on the MNPs for the fresh and reused catalysts was evaluated through ICP analysis, revealing a quantity of about 0.130 mmol/g and 0.123 mmol/g, respectively. Also, Fig. 11d shows magnetic property of reused catalyst is preserved after five runs.



**Scheme 3.** The suggested mechanism for the synthesis of the 2-amino-4H-pyran derivatives in the presence of MCF@SiO<sub>2</sub>-Pr-ABT@ZnCl<sub>2</sub> MNPs.



**Scheme 4.** The suggested mechanism for the synthesis of the N-arylquinoline derivatives in the presence of MCF@SiO<sub>2</sub>-Pr-ABT@ZnCl<sub>2</sub> MNPs.

### 3.10. The proposed mechanism for synthesis of the 2-amino-4H-pyrans in the presence of MCF@SiO<sub>2</sub>-Pr-ABT@ZnCl<sub>2</sub>

The mechanism proposed for the synthesis of 2-amino-4H-pyrans by MCF@SiO<sub>2</sub>-Pr-ABT@ZnCl<sub>2</sub> as a catalyst is outlined in [Scheme 3](#). This process is initiated by a Knoevenagel condensation reaction between malononitrile and activated aldehyde with Lewis acid sites of MNPs (zinc groups), which gives intermediate (I) after the removal H<sub>2</sub>O. A Michael addition is then carry out between intermediate (I) and the enolized C–H activated of 4-hydroxycumarin. Subsequently, a cyclization process is performed by attack of the enolized C–H active acid on the nitrile group to produce intermediate (II). Finally, the imine-enamine tautomerization leads to the desired product [51]. Also, a similar mechanism is suggested for the synthesis of N-arylquinoline derivatives in the presence of MCF@SiO<sub>2</sub>-Pr-ABT@ZnCl<sub>2</sub> MNPs as catalyst and using the corresponding reactants ([Scheme 4.](#)) [27].

## 4. Conclusion

In this study Zn complexed on hybrid manganese doped cobalt ferrite nanoparticles covered by silica were synthesized via a simple method. The structure of these uniform spherical shape MNPs was identified by FT-IR, XRD, FE-SEM, EDS, VSM, ICP, Zeta potential and TGA techniques. The FE-SEM images showed different size distributions of NPs, which confirms the presence of aggregation in MNP structures. Also, The zeta potential analysis showed that the surface charge of MCF@SiO<sub>2</sub>-Pr-ABT@ZnCl<sub>2</sub> MNPs is negative

(about  $-1.19$  mV). The MCF@SiO<sub>2</sub>-Pr-ABT@ZnCl<sub>2</sub> MNPs showed a magnetic properties about 20 emu g<sup>-1</sup>. These MNPs were used as catalyst in the synthesis of 2-amino-4H-pyran and N- arylquinoline derivatives under optimal conditions. Some prominent advantages of this method include high yield of product, short reaction time, green conditions, easy workup, simple separation of nanocatalyst using the magnet, and reusability of NPs during five runs.

### CRedit authorship contribution statement

**Najmieh Ahadi:** Writing – review & editing, Writing – original draft, Investigation. **Akbar Mobinikhaledi:** Writing – review & editing, Supervision, Investigation. **Amir Hossain Ebrahimi:** Investigation.

### Declaration of competing interest

The authors declare the following financial interests/personal relationships which may be considered as potential competing interests:

Akbar Mobinikhaledi reports was provided by Arak University. Akbar Mobinikhaledi reports a relationship with Arak University that includes: employment. Akbar Mobinikhaledi has patent pending to: No patent. Authors have no relevant financial or non-financial interests to disclose. If there are other authors, they declare that they have no known competing financial interests or personal relationships that could have appeared to influence the work reported in this paper.

### Acknowledgment

We gratefully acknowledge the financial support of this work by the research council of Arak University.

### Appendix A. Supplementary data

Supplementary data to this article can be found online at <https://doi.org/10.1016/j.heliyon.2024.e30620>.

### References

- [1] S.B. Lagu, R.P. Yejella, S. Nissankarara, R.R. Bhandare, V.S. Golla, B.V. Subrahmanya Lokesh, M.M. Rahman, A.B. Shaik, Antitubercular activity assessment of fluorinated chalcones, 2-aminopyridine-3-carbonitrile and 2-amino-4H-pyran-3-carbonitrile derivatives: in vitro, molecular docking and in-silico drug likeliness studies, *PLoS One* 17 (2022) e0265068, <https://doi.org/10.1371/journal.pone.0265068>.
- [2] M.M. Elbadawi, W.M. Eldehna, A.A. Abd El-Hafeez, W.R. Somaa, A. Albohy, S.T. Al-Rashood, K.K. Agama, E.B. Elkaeed, P. Ghosh, Y. Pommier, 2-Arylquinolines as novel anticancer agents with dual EGFR/FAK kinase inhibitory activity: synthesis, biological evaluation, and molecular modelling insights, *J. Enzym. Inhib. Med. Chem.* 37 (2022) 355–378, <https://doi.org/10.1021/om00075a013>.
- [3] H. Hussain, S. Aziz, B. Schulz, K. Krohn, Synthesis of a 4H-anthra [1, 2-b] pyran derivative and its antimicrobial activity, *Nat. Prod. Commun.* 6 (2011) 1934578X1100600621, <https://doi.org/10.1177/1934578X1100600621>.
- [4] S. Janeoo, H. Kaur, G. Kaul, A. Akhbir, S. Chopra, S. Banerjee, V. Kumar, R. Kumar, Fluorine-containing 2, 3-diaryl quinolines as potent inhibitors of methicillin and vancomycin-resistant *Staphylococcus aureus*: synthesis, antibacterial activity and molecular docking studies, *J. Mol. Struct.* 1244 (2021) 130924–130935, <https://doi.org/10.1016/j.molstruc.2021.130924>.
- [5] G. Grygoriv, D. Lega, L. Shemchuk, L. Maloshtan, G. Kalenichenko, V. Chernykh, L. Shemchuk, The synthesis of 2-amino-4-aryl-4H-pyrano [3, 2-c][1, 2] benzoxathiine-3-carbonitrile 5, 5-dioxides and the study of their effect on the blood coagulation process, *News of Pharmacy* (2018) 3–8, <https://doi.org/10.24959/nphj.18.2224>.
- [6] A.S. Waghmare, S.S. Pandit, D.M. Suryawanshi, DABCO catalyzed green and efficient synthesis of 2-Amino-4H-Pyrans and their biological evaluation as antimicrobial and anticancer agents, *Combin. Chem.* 21 (2018) 254–261, <https://doi.org/10.2174/1386207321666180315095422>.
- [7] R. Mohammadi, S. Esmati, M. Gholamhosseini-Nazari, R. Teimuri-Mofrad, Novel ferrocene substituted benzimidazolium based ionic liquid immobilized on magnetite as an efficient nano-catalyst for the synthesis of pyran derivatives, *J. Mol. Liq.* 275 (2019) 523–534, <https://doi.org/10.1016/j.molliq.2018.11.042>.
- [8] A. Maleki, M. Azizi, Z. Emdadi, A novel poly (ethyleneoxide)-based magnetic nanocomposite catalyst for highly efficient multicomponent synthesis of pyran derivatives, *Green Chem. Lett. Rev.* 11 (2018) 573–582, <https://doi.org/10.1080/17518253.2018.1547795>.
- [9] D. Das, Multicomponent reactions in organic synthesis using copper-based nanocatalysts, *ChemistrySelect* 1 (2016) 1959–1980, <https://doi.org/10.1002/slct.201600414>.
- [10] X.-S. Wang, M.-M. Zhang, H. Jiang, C.-S. Yao, S.-J. Tu, Three-component green synthesis of N-arylquinoline derivatives in ionic liquid [Bmim+][BF4-]: reactions of arylaldehyde, 3-arylamino-5, 5-dimethylcyclohex-2-enone, and active methylene compounds, *Tetrahedron* 63 (2007) 4439–4449, <https://doi.org/10.1016/j.tet.2007.03.068>.
- [11] S. Gao, C.H. Tsai, C. Tseng, C.-F. Yao, Fluoride ion catalyzed multicomponent reactions for efficient synthesis of 4H-chromene and N-arylquinoline derivatives in aqueous media, *Tetrahedron* 64 (2008) 9143–9149, <https://doi.org/10.1016/j.tet.2008.06.061>.
- [12] Z.-J. Yang, Q.-T. Gong, Y. Wang, Y. Yu, Y.-H. Liu, N. Wang, X.-Q. Yu, Biocatalytic tandem multicomponent reactions for one-pot synthesis of 2-Amino-4H-Pyran library and in vitro biological evaluation, *Mol. Catal.* 491 (2020) 110983–111107, <https://doi.org/10.1016/j.mcat.2020.110983>.
- [13] E. Kolvari, N. Koukabi, Z. Ozmaei, H. Khoshkho, F. Seidi, Synthesis of 2-amino-4H-pyran and 2-benzylidene malononitrile derivatives using a basil seed as a cheap, natural, and biodegradable catalyst, *Curr. Res. Green Sustain. Chem.* 5 (2022) 100327–100340, <https://doi.org/10.1016/j.crgsc.2022.100327>.
- [14] M.G. Dekamin, S.Z. Peyman, Z. Karimi, S. Javanshir, M.R. Naimi-Jamal, M. Barikani, Sodium alginate: an efficient biopolymeric catalyst for green synthesis of 2-amino-4H-pyran derivatives, *Int. J. Biol. Macromol.* 87 (2016) 172–179, <https://doi.org/10.1016/j.ijbiomac.2016.01.080>.
- [15] N. Zahin, R. Anwar, D. Tewari, M.T. Kabir, A. Sajid, B. Mathew, M.S. Uddin, L. Aleya, M.M. Abdel-Daim, Nanoparticles and its biomedical applications in health and diseases: special focus on drug delivery, *Environ. Sci. Pollut. Res.* 27 (2020) 19151–19168, <https://doi.org/10.1007/s11356-019-05211-0>.
- [16] P. Rath, S. Behera, B. Priyadarshini, S. Panda, D. Mandal, T. Sahoo, S. Mishra, T.R. Sahoo, P. Parhi, Influence of Mg doping on ZnO NPs for enhanced adsorption activity of Congo Red dye, *Appl. Surf. Sci.* 491 (2019) 256–266, <https://doi.org/10.1016/j.apsusc.2019.06.120>.
- [17] X. Li, J. Wei, K.E. Aifantis, Y. Fan, Q. Feng, F.Z. Cui, F. Watari, Current investigations into magnetic nanoparticles for biomedical applications, *J. Biomed. Mater. Res. A* 104 (2016) 1285–1296, <https://doi.org/10.1002/jbm.a.35654>.

- [18] S. Wang, Z. Sun, Y. Hou, Engineering nanoparticles toward the modulation of emerging cancer immunotherapy, *Adv. Healthcare Mater.* 10 (2021) 2000845–2000878, <https://doi.org/10.1002/adhm.202000845>.
- [19] M.J. Ndolomingo, N. Bingwa, R. Meijboom, Review of supported metal nanoparticles: synthesis methodologies, advantages and application as catalysts, *J. Mater. Sci.* 55 (2020) 6195–6241, <https://doi.org/10.1007/s10853-020-04415-x>.
- [20] O. Dlugosz, K. Szostak, A. Staroń, J. Pulit-Prociak, M. Banach, Methods for reducing the toxicity of metal and metal oxide NPs as biomedicine, *Materials* 13 (2020) 279–298, <https://doi.org/10.3390/ma13020279>.
- [21] M.A. Bodaghifard, M. Hamidinasab, N. Ahadi, Recent advances in the preparation and application of organic–inorganic hybrid magnetic nanocatalysts on multicomponent reactions, *Curr. Org. Chem.* 22 (2018) 234–267, <https://doi.org/10.2174/1385272821666170705144854>.
- [22] L. Xu, Z. Zhu, D.-W. Sun, Bioinspired nanomodification strategies: moving from chemical-based agrosystems to sustainable agriculture, *ACS Nano* 15 (2021) 12655–12686, <https://doi.org/10.1021/acsnano.1c03948>.
- [23] D.S. Aher, K.R. Khillare, L.D. Chavan, S.G. Shankarwar, Quaternary vanado-molybdotungstophosphoric acid [H5PW6Mo4V2O40] over natural montmorillonite as a heterogeneous catalyst for the synthesis 4H-pyran and polyhydroquinoline derivatives, *ChemistrySelect* 5 (2020) 7320–7331, <https://doi.org/10.1002/slct.202001065>.
- [24] A. Mobinikhaledi, N. Ahadi, M. Haseli, The use of MnCoFe2O4@ GT@ Cu magnetic nanoparticles in the synthesis of benzopyrans, *Org. Prep. Proced. Int.* 54 (2022) 465–472, <https://doi.org/10.1080/00304948.2022.2085985>.
- [25] N. Ahadi, M.A. Bodaghifard, A. Mobinikhaledi, Preparation and characterization of a novel organic–inorganic hybrid nanostructure: application in synthesis of spirocompounds, *Res. Chem. Intermed.* 46 (2020) 3277–3294, <https://doi.org/10.1007/s11164-020-04130-x>.
- [26] A. Mobinikhaledi, N. Foroughifar, H. Moghanian, N. Keshavarzi, Piperazine catalyzed convenient synthesis of 4H-pyran derivatives from  $\alpha$ ,  $\alpha'$ -bis (substituted-benzylidene) cycloalkanones and malononitrile under reflux conditions, *J. Saudi Chem. Soc.* 19 (2015) 399–403, <https://doi.org/10.1016/j.jscs.2012.05.001>.
- [27] N. Ahadi, A. Mobinikhaledi, M.A. Bodaghifard, One-pot synthesis of 1, 4-dihydropyridines and N-arylquinolines in the presence of copper complex stabilized on MnFe2O4 (MFO) as a novel organic–inorganic hybrid material and magnetically retrievable catalyst, *Appl. Organomet. Chem.* 34 (2020) e5822, <https://doi.org/10.1002/aoc.5822>.
- [28] N. Ahadi, A. Mobinikhaledi, R.M. Hosseini, An application study of MnCoFe2O4@ PEG-4000 (MCF@ PEG-4000) MNPs as a catalyst in the synthesis of hexahydroquinolines and benzopyrans and as a nano-adsorbent for the removal of Cu (II) and Fe (III) ions in aqueous solutions, *J. Nanoparticle Res.* 25 (2023) 46–61, <https://doi.org/10.1007/s11051-023-05689-3>.
- [29] R. Rahimizadeh, A. Mobinikhaledi, H. Moghanian, S.S. Kashaninejad, Design and synthesis of some new biologically active amidoalkyl naphthols in the presence of sulfonic acid functionalized silica-coated Fe3O4 nanoparticles, *Res. Chem. Intermed.* (2021) 1–21, <https://doi.org/10.1007/s11164-021-04610-8>.
- [30] N. Ahadi, A. Mobinikhaledi, A. Fathehesami, Z. Bagheri, Zn salen complex supported on MnCoFe2O4 (MCF) magnetic nanoparticles as a catalyst in the synthesis of 3, 4-dihydropyrimidin-2 (1H)-ones/thiones (Biginelli-like reaction), *Res. Chem. Intermed.* 48 (2022) 2469–2488, <https://doi.org/10.1007/s11164-022-04709-6>.
- [31] A. Yanti Kiding, Sudarmono, T. Octolia, Synthesis and characterization of activated carbon from sago waste (metroxyton sago) with ZnCl2 activation and HNO3 modification, *J. Indones. Chem. Soc.* 2 (2019) 48–53, <https://doi.org/10.34311/jics.2019.02.1.48>.
- [32] G. Datt, A. Abhyankar, Dopant driven tunability of dielectric relaxation in MxCo (1-x) Fe2O4 (M: Zn2+, Mn2+, Ni2+) nano-ferrites, *J. Appl. Phys.* 122 (2017) 1–11, <https://doi.org/10.1063/1.4990275>.
- [33] M. Zainuri, Hematite from natural iron stones as microwave absorbing material on X-band frequency ranges 1 (2017), 012008-012013. doi: 0.1088/1757-899X/196/1/012008.
- [34] L. Al-Harbi, M.S. Darwish, Functionalized iron oxide nanoparticles: synthesis through ultrasonic-assisted co-precipitation and performance as hyperthermic agents for biomedical applications, *Heliyon* 8 (2022) e09654, <https://doi.org/10.1016/j.heliyon.2022.e09654>.
- [35] V. Alimohammadi, S.A. Seyyed Ebrahimi, F. Kashanian, Z. Lalegani, M. Habibi-Rezaei, B. Hamawandi, Hydrophobic magnetite nanoparticles for bioseparation: green synthesis, functionalization, and characterization, *Magnetochemistry* 8 (2022) 143–157, <https://doi.org/10.3390/magnetochemistry8110143>.
- [36] F.K. Cartledge, Steric effects on reactivity in silicon chemistry, *Organometallics* 2 (1983) 425–430.
- [37] N. Sulaiman, M. Ghazali, J. Yunas, A. Rajabi, B. Majlis, M. Razali, Synthesis and characterization of CaFe2O4 nanoparticles via co-precipitation and auto-combustion methods, *Ceram. Int.* 44 (2018) 46–50, <https://doi.org/10.1016/j.ceramint.2017.08.203>.
- [38] M. Omid, A. Mobinikhaledi, Sulfonic acid pyridinium chloride-functionalized nanoparticles (MnCoFe2O4@ Niacin-SO3H)+ Cl<sup>-</sup> as a novel and reusable catalyst for synthesis of tetrahydropyrazolopyridines and pyranopyrazoles, *Res. Chem. Intermed.* 48 (2022) 4347–4371, <https://doi.org/10.1007/s11164-022-04800-y>.
- [39] E. Jahangard, L. Khazdooz, A. Zarei, Synthesis and in vitro antibacterial study of dihydropyran [3, 2-c] chromene derivatives by nano fluoro apatite doped with Mg and Si as a cooperative catalyst, *Iran. J. Catal.* 10 (2020) 57–63.
- [40] M. Khaleghi-Abbasabadi, D. Azarifar, Magnetic Fe3O4-supported sulfonic acid-functionalized graphene oxide (Fe3O4@ GO-naphthalene-SO3H): a novel and recyclable nanocatalyst for green one-pot synthesis of 5-oxo-dihydropyran [3, 2-c] chromenes and 2-amino-3-cyano-1, 4, 5, 6-tetrahydropyran [3, 2-c] quinolin-5-ones, *Res. Chem. Intermed.* 45 (2019) 2095–2118, <https://doi.org/10.1007/s11164-018-03722-y>.
- [41] N. Noroozi Pesyran, G. Rezanejad Bardajee, E. Kashani, M. Mohammadi, H. Batmani, Ni (II)-Schiff base/SBA-15: a nanostructure and reusable catalyst for one-pot three-component green synthesis of 3, 4-dihydropyran [3, 2-c] chromene derivatives, *Res. Chem. Intermed.* 46 (2020) 347–367, <https://doi.org/10.1007/s11164-019-03954-6>.
- [42] N. Ahadi, M.A. Bodaghifard, A. Mobinikhaledi, Cu (II)- $\beta$ -cyclodextrin complex stabilized on magnetic nanoparticles: a retrievable hybrid promoter for green synthesis of spirocompounds, *Appl. Organomet. Chem.* 33 (2019) e4738, <https://doi.org/10.1002/aoc.4738>.
- [43] S. Asadpour Behzadi, E. Sheikhsosseini, S. Ali Ahmadi, D. Ghazanfari, M. Akhgar, Mefenamic acid as environmentally catalyst for three-component synthesis of dihydropyran [2, 3-c] chromene and pyran [2, 3-d] pyrimidine derivatives, *J. Appl. Chem.* 14 (2020) 63–73, <https://doi.org/10.1007/s11164-018-03722-y>.
- [44] S. Karami, A.R. Momeni, J. Albadi, Preparation and application of triphenyl (propyl-3-hydrogen sulfate) phosphonium bromide as new efficient ionic liquid catalyst for synthesis of 5-arylidene barbituric acids and pyran [2, 3-d] pyrimidine derivatives, *Res. Chem. Intermed.* 45 (2019) 3395–3408, <https://doi.org/10.1007/s11164-019-03798-0>.
- [45] T.L. Lambert, Microwave assisted solecic as heterogeneous catalyst for multicomponent one-pot synthesis of novel chromene scaffolds with quantitative yields, *J. Chin. Adv. Mater. Soc.* 6 (2018) 134–144, <https://doi.org/10.1080/22243682.2018.1426040>.
- [46] S.K. Singh, K.N. Singh, DBU-catalyzed expeditious and facile multicomponent synthesis of N-arylquinolines under microwave irradiation, *Monatsh. Chem.* 143 (2012) 805–808.
- [47] M. Fathabadi, B. Pouramiri, M. Zahedifar, H. Sheibani, K. Saidi, Polyaniline, polyaniline/SiO2 and poly (4-vinylpyridine): as highly efficient and recyclable green heterogeneous basic catalysts for the three-component synthesis of tetrahydrobenzopyran and 3, 4-dihydropyran [c] chromene derivatives, *Iran. J. Chem. Chem. Eng.* 40 (2021) 429–436.
- [48] M. Bhosle, D. Wahul, G. Bondle, A. Sarkate, S. Tiwari, An efficient multicomponent synthesis and in vitro anticancer activity of dihydropyranochromene and chromenopyrimidine-2, 5-diones, *Synth. Commun.* 48 (2018) 2046–2060, <https://doi.org/10.1080/00397911.2018.1480042>.
- [49] H. Mehrabi, H. Abusaidi, Synthesis of biscoumarin and 3, 4-dihydropyran [c] chromene derivatives catalysed by sodium dodecyl sulfate (SDS) in neat water, *J. Iran. Chem. Soc.* 7 (2010) 890–894, <https://doi.org/10.1007/BF03246084>.
- [50] T. Ahmadi, A. Monshi, V. Mortazavi, M. Fathi, S. Sharifi, B.H. Beni, A.M. Abed, M. Kheradmandfard, A. Sharifnabi, Synthesis and dissolution behavior of nanosized silicon and magnesium co-doped fluorapatite obtained by high energy ball milling, *Ceram. Int.* 40 (2014) 8341–8349, <https://doi.org/10.1016/j.ceramint.2014.01.040>.
- [51] M. Aghaei-Hashjin, A. Yahyazadeh, E. Abbaspour-Gilandeh, Zr@ IL-Fe3O4 MNPs as an efficient and green heterogeneous magnetic nanocatalyst for the one-pot three-component synthesis of highly substituted pyran derivatives under solvent-free conditions, *RSC Adv.* 11 (2021) 23491–23505, <https://doi.org/10.1039/D1RA04381A>.